A Novel Alginate and Expanded Graphite Based Composite for use in Solar and Waste Heat Storage

Jack Reynolds[1], Rhodri Williams[1], Jonathon Elvins[1] Eifion Jewell[1], Justin Searle[1] and Xinyuan Ke[2]

1 Swansea University, Swansea (United Kingdom)

2 University of Bath, Bath (United Kingdom)

Abstract

Thermochemical heat storage composites based on hydrated salts enclosed within an expanded graphite/alginate polymer matrix are presented. The simple synthesis method offers flexibility in the size and shape of the composite material to best suit the application, with the option of easily being scaled up. The incorporated calcium chloride can release and store heat through the reversible hydration and dehydration reaction. The Dehydration of the reacting salt is appropriate for sources of heat ranging from transpired conventional solar collectors (<70°C) up to low grade waste heat sources (<150°). Salt loading values up to 84% have been achieved while maintaining visible porosity. The charge reaction is studied via static heat, while the discharge reaction is studied by passing a flow of humid air through the materials. Both reactions are compared to previously studied Vermiculite/$CaCl_2$. Further to this bulk density, surface area, and water vapor sorption are considered.

Keywords: Thermochemical Heat Storage, Expanded Graphite, Alginate, Calcium Chloride

1. Introduction

With the exhaustion of our world's main fossil-based energy resources and the continued worsening of our environmental conditions in the past decades, it is vital we look to change the way we generate, use, and store our energy. In 2017, almost half the energy consumed (760 TWh) in the UK was required for heating purposes, of which 57% was needed for domestic space heating (Ofgem, 2016). For the heating of the UK's 29 million homes and non-residential buildings, only 4.5% of the energy was from a low carbon source, which needs to increase drastically if the UK is to meet its 2050 net carbon zero target (Ofgem, 2020; Climate Change Act 2008). Two low carbon sources associated with an abundance of heat energy are solar heat and industrial waste heat (IWH), however both come with inherent problems. Solar heat has a timing mismatch between when heat is abundant and when heat is required (diurnally and seasonally), whereas IWH heat can be discontinuous and has a distance mismatch between the source and the necessity. The solution to both these problems is effective heat storage.

Thermochemical heat storage (THS) provides a convenient way to overcome these mismatch issues by storing heat energy in a reversible endothermic reaction. The benefits of THS over sensible heat storage (SHS) and latent heat storage (LHS) is its superior theoretical energy density and its ability to store heat energy indefinitely, which the two latter options cannot (Jarimi et al, 2019). Sorption heat storage has been utilized for both mobile THS, transporting IWH to an off-site heat demand, and for inter-seasonal heat storage at the demand location (Krönauer et al, 2015; Krese et al, 2018). The most popular sorption TCS materials in literature are 'Salt in Matrix' or SIM (Casey et al, 2015; Mohapatra and Nandanavanam, 2022; Brancato et al, 2021). Here, the enthalpy of the reversible hydration reaction of the salt is used to store energy within a physical scaffolding. The matrix provides a large surface (to aid the sorption kinetics) and high porosity while also acting as a protective structure to mitigate the problems of deliquescence and salt leakage (Sutton et al, 2018). Examples of typical materials used for this are vermiculite (Brancato et al, 2021), silica gel (Courbon et al, 2017), activated alumina (Zhang et al, 2018), activated carbon (Casey et al, 2015) and expanded graphite (Salviati et al, 2019). The latter is used for its low price and density, high surface area and associated higher thermal conductivity compared to other options. While the results are promising, expectations for the resulting composites in terms of energy density and cycle stability are rarely met due to lower bulk densities, agglomeration, and salt leakage (Clark et al, 2020). Recently, hybrid salt/expanded graphite have been prepared in a pellet form with additions of an organic polyelectrolyte (Salviati et al, 2019) and ethyl cellulose (Gaeini

doi:10.18086/eurosun.2022.13.19 Available at http://proceedings.ises.org

et al, 2018) to mitigate some of these problems. Both studies showed improvements in cycle stability in the presence of these additives due to the reduced leakage of salt and even a positive contribution to reaction kinetics. However, utilizing expanded graphite in pellet form would decrease its internal porosity thus preventing sufficient passage of air through the composite like vermiculite. A freeze-drying technique has been employed to create a porous structure to contain the salt hydrate, strontium bromide, using expanded graphite and nanocellulose (Salviati et al, 2020). Hydration kinetics were shown to improve by 54% compared to the stand-alone salt hydrate which was accredited to its highly porous structure. More recently there has been some work involving the use of sodium alginic acid as a host matrix due to its excellent features of microscopic shaping (Kallenberger and Fröba, 2018; Kallenberger et al, 2018). In the presence of a divalent cation such as Ca^{2+} or Sr^{2+}, two Na^{+} cations already present are displaced and crosslinking in the polymer occurs (gelation). The divalent cations coordinate to oxygen atoms from different polymer chains resulting in the formation of a stable hydrogel. With this process it is possible to make controllable shapes such as spherical beads. High loading of thermochemically active salts within the matrix has been achieved with storage densities upwards of 417 kWh/m^3 (Kallenberger et al, 2018). This alginate derived matrix is a passive host and does not comprise of any micro or mesoporosity unlike more the commonly utilized matrices.

Here, we present a novel approach to combine expanded graphite, for its high surface area and thermal conductivity, with alginate-based polymers for their ease of microscopic shaping, to achieve a highly porous and stable network to hold thermochemically active salts. To best of our knowledge this is the first time that these two materials have been successfully combined and used as a matrix for thermochemical heat storage applications. $CaCl_2$ has been chosen as the incorporated salt due to its ability to act as both the 'gelation salt' and the thermally active material, while also showing superior storage capabilities compared to other salt options. It also benefits from being low cost, appropriate for low and higher temperature charging, and readily reacts with moisture to release energy (Gaeini et al, 2018; Walsh et al, 2020).

2. Materials and Methods

2.1. Materials

Calcium chloride was purchased from Sigma-Aldrich® in its dehydrated form and the saturated solution was made at room temperature. Sodium alginate in powder form was purchased from Sigma-Aldrich®. Expandable graphite grade BLG300L-LT, with an expansion start temperature of 140-160°C was purchased from RMC Reason GmbH (Bad Säckingen, Germany). To obtain expanded graphite (EG), flake samples were heated at >200°C for 1h. Expanded natural graphite (mEG) in milled form, with 25m^2/g surface area (as reported in the material data sheet) was purchased from Imerys Graphite & Carbon (Bironico, Switzerland), commercial grade TIMREX® C-THERM012.

2.2. Composite Synthesis

Two different synthesis routes are depicted in Fig. 1. Alginate solution is formed using a ratio of 1g of alginate to 50ml of water. This is stirred at 80°C until fully dissolved. The graphite is then added to solution at varied ratios. Method 1 requires dropwise addition of the Alginate/EG solution into a saturated calcium chloride solution to allow cross-linkage between Ca^{2+} ions and the alginate polymer. This mixture is stirred until all solution is transferred. Once complete the formed beads are left in solution for >24h before being filtered and dried at 120°C for a further 24h. Method 2 allows more control over the size of the beads by transferring Alginate/EG solution to a mould of a specific size. This is the kept at -20°C for >2h to allow adequate solidification of the beads. These are then transferred to the saturated calcium chloride solution for cross-linking and impregnation over a 24h period. Once complete these are filtered and dried at 120°C. The 3-4mm and 6mm diameter beads produced via method 1 and method 2 respectively are shown in Fig. 2.

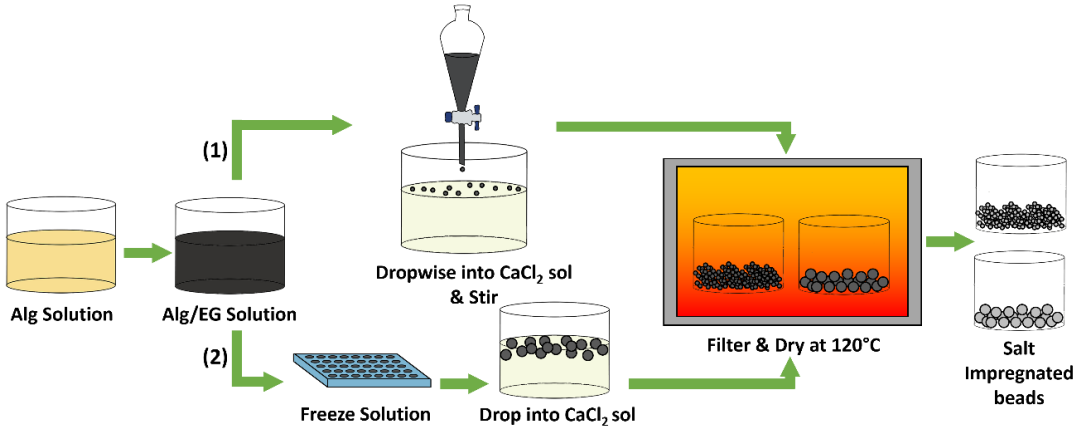

Fig. 1: Schematic illustration of fabrication of $CaCl_2$ impregnated Alg/EG beads 1) Dropwise method. 2) Freeze method

The choice of expanded graphite (mEG or EG) used in SIM synthesis results in completely different bead structure. This is highlighted in the SEM images shown in Fig. 3. The mEG beads show a large quantity of small pores on the surface, whereas the EG beads show much larger features. These consist of a few large surface pores, mostly filled with the impregnated salt. Surface porosity can have a large effect on reaction kinetics and cyclic stability. This is based on the ease of the reacting air reaching the salt and the ability of the salt to leak from the matrix. The size of the bead is dictated by the method of synthesis. Method 1 form beads in the range of -4mm, whereas for Method 2 the synthesized beads are greater than 6mm. The size of the formed beads effects the packing density, bulk density, and flow of reacting air. Smaller beads will increase the bulk density in a packed bead however will restrict the flow of air through the material. Salt loading can be controlled by the concentration of $CaCl_2$ in the gelation bath. All these parameters ultimately control the performance of the SIM during the charge and discharge cycles and the optimum synthesis parameters are to be found.

Tab. 1: Summary of Synthesized Composites

Sample	Method	Size	Expanded Graphite	EG:Alg
mEG-D	Drop Cast	3-4mm	C-Therm012	3:1
mEG-M	Mould	6mm	C-Therm012	6:1
EG-M	Mould	6mm	BLG300-LT	6:1
V-$CaCl_2$	Incipient Wetness	2-7mm	-	-

Fig. 2: Optical Images of synthesized beads. A) mEG-M. B) EG-M. C) mEG-D.

3. Characterization

The composite beads internal morphology was examined with a Zeiss Evo LS25 scanning electron microscope (SEM) with a 15kV accelerating voltage. The salt loading of the composites was determined from the analysis of chloride ion concentration by titration (Mohr's Method). The composite is washed in DI water for >1hour dissolving all the $CaCl_2$ that is present. This solution is then titrated against silver nitrate solution in the presence of a potassium chromate indicator. The bulk density of the sample was calculated from their mass reading (measured on a Ohaus Scout STX223 with a readability of 0.001g) in a known volume of a cylindrical container. The volume of the container is calculated from the filled mass of water ($1g=1cm^3$). The Micrometrics Tristar II 3020 is used to calculate the surface area of the of the porous structures by combining N_2 physisorption and BET analysis. Samples were dried prior to analysis using a micrometric VapPrep 061, which allowed samples to be degassed with nitrogen at 120°C for >12h. The charge performance was investigated using a Ohaus MB120 moisture analyser using a static drying profile. Prior to experiments, samples were subject to 30°C and 20%RH for >168h to achieve a uniform hexahydrate state. 5g of each sample were then subject to three different drying temperatures (120°C, 150°C & 200°C). To measure the discharge performance of the composites, a custom-built assembly is used (Fig.3). Prior to testing, materials are dried at 120°C for >24h to ensure the anhydrous state is achieved. Moist air is produced via a Cellkraft P-50 relative humidity generator. The flow of air is then fed into a reactor with a fixed volume of material. Temperature uplift and bulk temperature is calculated through a series of three thermocouples. Mass recordings are taken using three load cells situated at the base of the reactor. The water sorption kinetics of the composite beads were assessed via dynamic (water) vapor sorption (DVS) within the relative humidity range of 0 %–95 % at 25 °C, using the DVS Advantage instrument (Surface Measurement Systems). One bead was used for each test and the sample was stabilized at 0% RH before starting the water adsorption isotherm. For Static Vapor Sorption (SVS) tests, materials are dried at 120°C for >24h to ensure the anhydrous state is achieved. To add moisture evenly to the materails, a Memmert constant climate chamber HPP110eco is used. 3 petri dishes, each containing 10g of material, were subject to the three choosen relative humidity conditions (25%, 50% and 75% RH at 25°C) and left for 168 hours to assess the maximum water uptake. Mass recordings were taken every 24 hours.

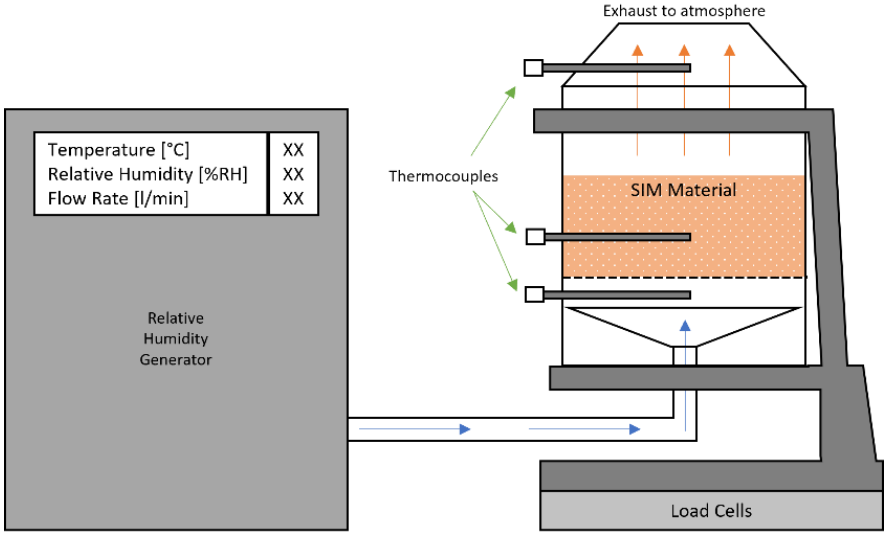

Fig. 3: Schematic of the experimental apparatus developed to investigate the discharge performance of typical thermochemical materials.

4. Results & Discussion

4.1. Morphological Analysis

The morphology of the bead composites was investigated by means of SEM. Fig. 4 reports the representative micrographs highlighting the surface and internal structures. The samples prepared with mEG clearly show the formation of beads with smaller pores and a large network of graphite scaffolding. Fig. 4d-f highlights a clear difference in the structure of $CaCl_2$ crystals inside the beads. The mEG samples form very small $CaCl_2$ crystals,

whereas the much larger structures present in EG seem to be completely covered in uniform layers. The presence of smaller crystals structures is advantageous as it enhances the contact area between a carrier gas and the salt. On the contrary, the smaller network of pores could cause restrictions from removing/adding moisture in the beads, leading to lower reaction kinetics.

As stated in previous work done by Sutton, N_2 physisorption can be considered in-accurate for the analysis of macro-porous material, however it is still suitable for the comparison between microporous materials. The surface area results are shown in Table 2. All graphite/alginate-based composites show a larger surface area than the previously studied V-$CaCl_2$. This indicates that these types of materials all form smaller crystal structures in their highly porous scaffolding, The two mEG samples have greatest surface area, which would be attributed to high surface area of the mEG giving a larger space for the salt to crystalize. Of these two samples the moulded beads show a higher surface area. This could be because of the larger mEG:Alginate ratio allowing more space for the salt to crystalise on the graphite surface. Alternatively, this could also be attributed to the freezing nature incorporated into the mould method. The freezing of solution may allow more time for the scaffolding to solidify before the melting, maintaining a larger network of pores.

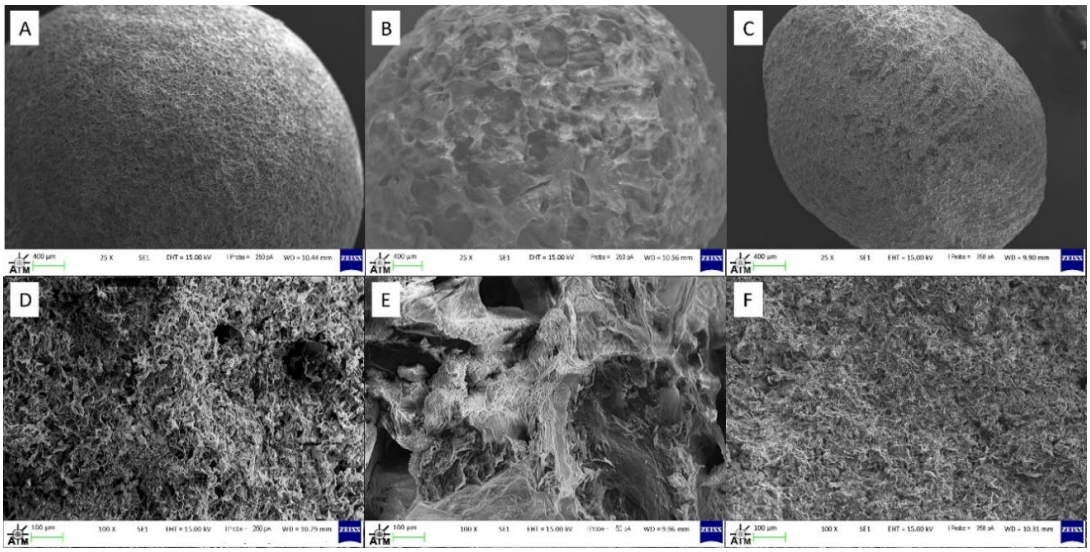

Fig. 4: SEM images showing the surface and internal structures of mEG-M (A,D), EG-M (B,E) and mEG-D (C,F) beads. A-C show surface structure. D-F show the bead cross-section.

Results from the Bulk density tests are shown in Table 2. Here we can see that the graphite alginate beads have a higher bulk density that previously studied V-$CaCl_2$. The highest of the three samples is the mEG-D beads which is expected due to the reduced diameter of the beads allowing the beads to fill more of the void fraction available in a given space. This could be beneficial to obtain more salt per unit of volume, however the resulting restriction of the carrier gas may have a negative impact on material performance. Of the two the mould samples, the mEG samples have a larger bulk density probably due to the higher surface area allowing more salt to be incorporated. This indicates a larger of amount of 'Matrix' material present per unit of volume.

4.2. Salt Characterization

Results from the Mohr's titration (Table 2) indicate the salt loading values for the expanded graphite materials are all higher than the V-$CaCl_2$ samples when salt content is based on the anhydrous state. Even with the addition of graphite, the composites can still achieve the high levels of salt loading which were observed with a pure alginate matrix (Kallenberger et al, 2018). Combining the Salt wt% and the bulk density values, we can estimate the salt volumetric density. From previous work on $CaCl_2$, we know the value of density (1830kg/m^3) and theoretical storage density (1.47 GJ/m^3) for the anhydrous state (Barreneche et al, 2015). Combining these values with the salt volumetric density value of our materials we can estimate the maximum theoretical storage density. The results show that mEG-D and mEG-M have around 3.5 and 2.5 more energy storage capabilities than V-$CaCl_2$.

Tab. 2: Physical characteristics of the Synthesized Materials.

Sample	Salt Loading [%]	Bulk Density [g/cm^3]	Salt Volumetric Density [g/cm^3]	Theoretical Storage Density [MJ/m^3]	Surface Area [m^2/g]
mEG-D	78	0.777	0.606	486.8	4.02
mEG-M	84	0.547	0.459	368.7	4.49
EG-M	72	0.365	0.263	211.3	2.80
V-$CaCl_2$	66	0.263	0.174	139.7	1.59

4.3. Water Sorption

A DVS isotherm conducted on the mEG-M and EG-M samples is shown in Fig. 5. Both samples start to take up water from around 30-35%RH then following a similar trend up to the same mass gain of 120wt% at 90%RH. This is characteristic of CaCl2 reaching its maximum hydrated state and slightly beyond. As the RH approaches 95% the materials begin to act differently. The EG-M sample rapidly increases to a 160wt% gain, whereas mEG-M sample flattens off. This suggests that the larger pores in the EG sample allow deliquescence to take place throughout the samples, whereas deliquescence occurring in the smaller pores at the surface of mEG may restrict this phenomenon throughout. As for the desorption cycle, the EG sample begins to lose water at 60% RH whereas the mEG sample doesn't begin to lose water until below 15% RH. The significant desorption hysteresis observed from both samples suggest the presence of ink-bottle type pore structure (Morishige and Tateishi, 2003) in consistent with the results shown in the SEM images and surface topography images. This also suggests that the water is easier desorbed from the material with the largest pores. In the mEG sample, the small pores may become blocked from salt block-ages close to the edge of the beads.

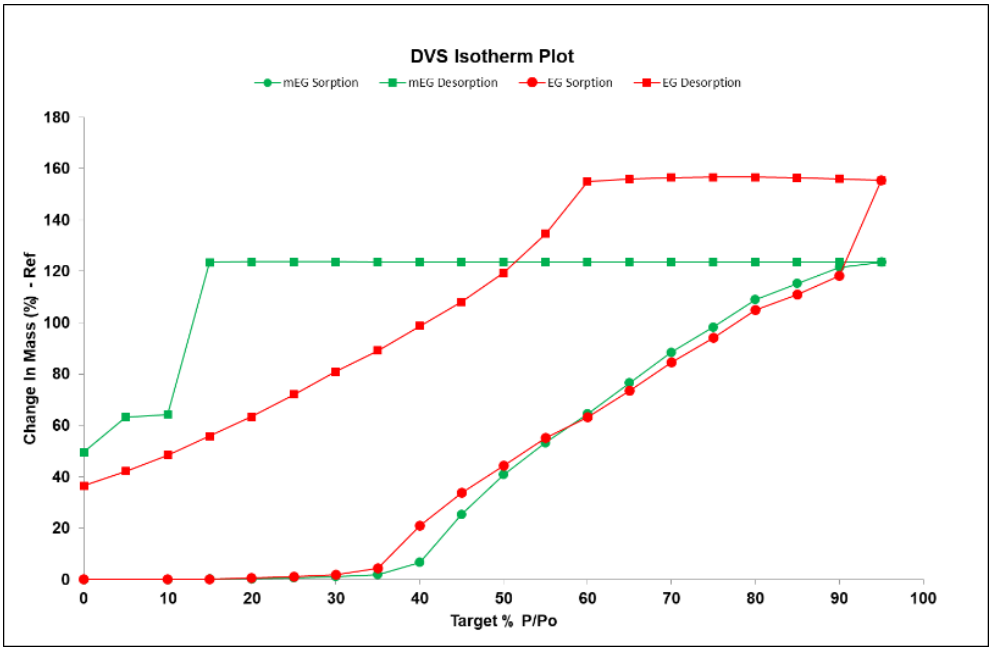

Fig. 5: DVS Isotherm of samples mEG-M and EG-M.

The raw SVS results and water uptake per unit volume data is shown in Fig. 6. The relative humidity values chosen were 25%, 50% and 75%. All conditions were conducted at 25°C. Interrogating the raw data, all four

materials take up moisture at a very similar rate over 24hrs. This is because unreacted salt is more easily accessible during this time frame, being close or directly on the surface of the aggregates. Beyond 24hrs, either the quantity of salt available or the kinetics of moisture transfer through the aggregates differentiates their uptake. For the lower RH%, the vermiculite and mEG-D samples show superior water uptake. This is because more of the salt is considered surface salt in vermiculite and the bead diameter is much smaller for mEG-D, reducing the distance for moisture transport. The shape of mEG-M and EG-M curves at this RH and the known salt wt% values suggest water uptake is not complete after 7 days for these samples. For the 50% and 75% conditions, the quantity of salt dominates the performance of the materials after 24 hrs. This is because the kinetics of moisture transport are much higher under these conditions. In both cases the quantity of moisture uptake aligns with the salt wt% of the materials. When looking at moisture uptake per unit volume, by considering the bulk density, we can see that all EG/Alg materials take up more water than V-CaCl2 on both the 24hr and 7-day period (Fig. 7). Interestingly, the mEG-M performs better than the mEG-D even though the latter has a higher salt volumetric density. This suggests that more salt is accessible in the moulded sample due to a higher surface area or larger network of internal pores.

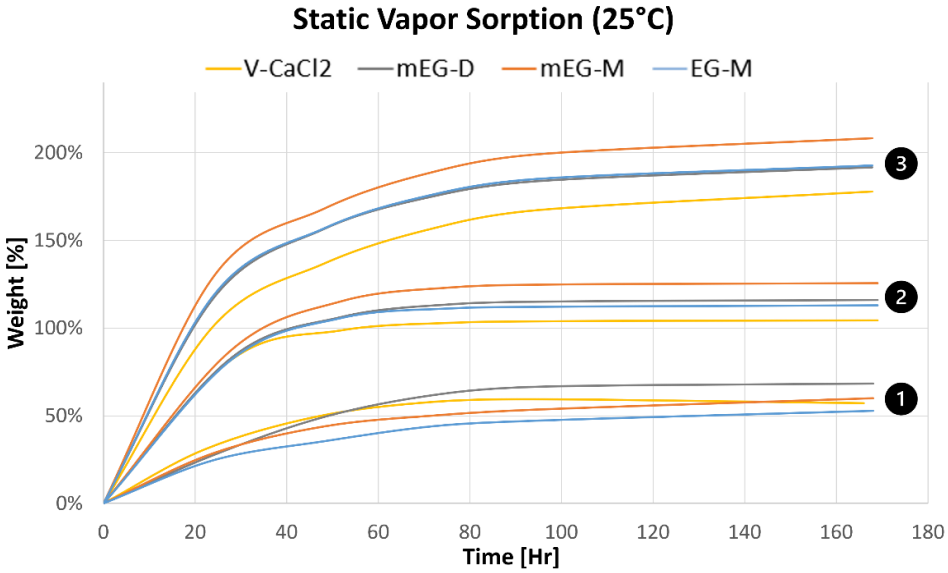

Fig. 6: SVS Analysis of all four samples at 25% (1), 50% (2) & 75% (3) RH.

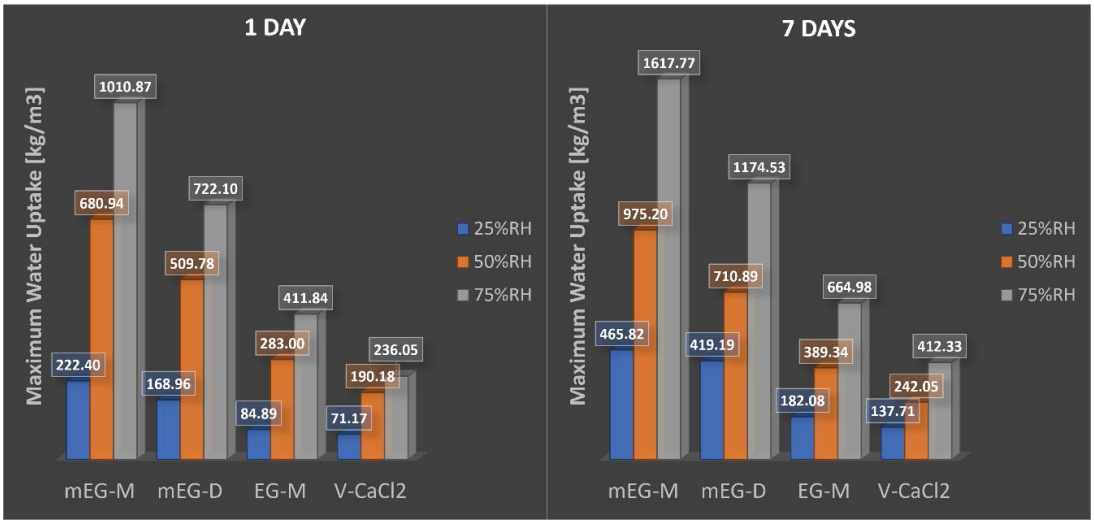

Fig. 7: Water uptake per volume of material over 1 day and 7 days.

4.4. Thermal Properties

To evaluate the thermal response of all the materials, each was placed inside the vertical cylindrical reactor with the air entering at the base (Fig.3). For each experiment, the reactor was loaded with 200cm^3 of material. To create a flow of air with consistent and controllable parameters, a Cellkraft P-50 relative humidity generator is used. The chosen conditions for the experiments were 60%RH, 20 l/min, 25°C for a duration of 3 hours. Fig. 8 shows the response of the materials to the given conditions. All four materials successfully release the chemically stored heat energy when subjected to moisture in the air flow.

Although the initial temperature spike varies slightly between samples, all the material act very similar. This is because there is only a certain amount of moisture being delivered in the flow of air. The mass data shows that all four materials take up moisture at the same rate owing to the equivalent amount of $CaCl_2$ being accessible for absorption over the 3-hour cycle. Knowing that, the energy output is expected to be similar. The initial spike in temperature for V-$CaCl_2$ would be characteristic of more salt available on the surface of material. As for the mEG-M sample, it is believed that there is good air flow through the packed bed because of the uniform spherical shape. This postulated the lower peak in mEG-D, as the smaller beads lead to tighter packing restricting air flow.

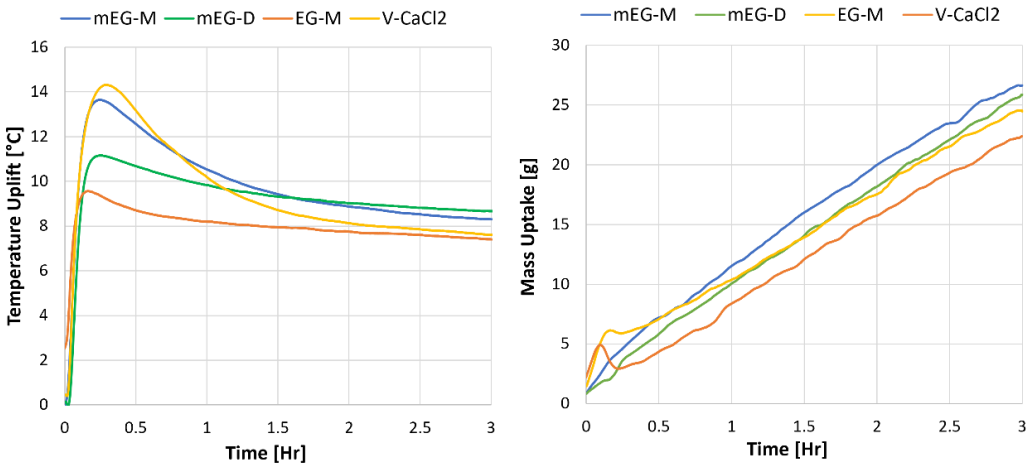

Fig. 8: Discharge results for each material. Temperature uplift from inlet to outlet (Left). Moisture uptake (Right).

Tab. 3: Estimation of reaction progression of each material based on the mass of CaCl2 and water uptake.

Sample	Volume of Material [cm^3]	Mass of $CaCl_2$ [g]	Hexahydrate Mass Uptake [g]	Reaction %
mEG-D	200	121.2	118.0	21
mEG-M	200	91.8	89.4	28
EG-M	200	52.6	51.2	49
V-$CaCl_2$	200	34.8	33.9	74

Thermal transfer will preferentially heat the localized walls of the reactor as opposed to quick initial heat release. The EG-M sample having the lowest peak maximum temperature is a consequence of lower salt, lower surface area, and harder to reach internal salt. All four materials gradually begin to reduce to a lower/ plateaued temperature uplift over time. This is expected because the energy associated with transitions from anhydrous to the dihydrate state is higher than the dihydrate/tetrahydrate to hexahydrate state. Over time, less anhydrous $CaCl_2$ is available and so less heat will be evolved. On top of this the kinetics of moisture uptake will reduce as the moisture will now have to travel to harder to reach places in the aggregates. Lowering the kinetics will directly affect the temperature uplift. Even considering this the EG/Alg materials still maintain

a good uplift after three hours with no direct sign of decreasing. To understand the reaction progression, we can take the moisture uptake value and compare this to the theoretical mass uptake to achieve a uniform hexahydrate state. Table 3 highlights the amount of $CaCl_2$ available for each experiment and the amount of water needed to reach the maximum hydrated state. To calculate to reaction %, a presumption that all materials have absorbed 25g of water is used. The results show that all EG/Alg materials have far more energy to release than V-$CaCl_2$. On this calculation it can be estimated that $CaCl_2$ has around 1hour left before reaction completion is achieved. As for mEG-D, mEG-M and EG-M, we can estimate they have around 12hrs, 9hrs and 3hrs left respectively.

Dehydration studies under static temperature conditions at 120°C, 150°C and 200°C are shown in Fig. 9. Mass data is logged until a variation of less than +/- 1mg change is observed for 120 seconds. In all three cases V-$CaCl_2$ has a higher rate of dehydration which is characteristic of the salt being spread over a much larger volume. Of the three expanded graphite materials, mEG-M shows the slowest rate. This is due to the larger spherical shape (larger distance for moisture transport) than mEG-D, and smaller structural porosity than EG-M. This agrees with the results shown from the desorption curves of the DVS analysis.

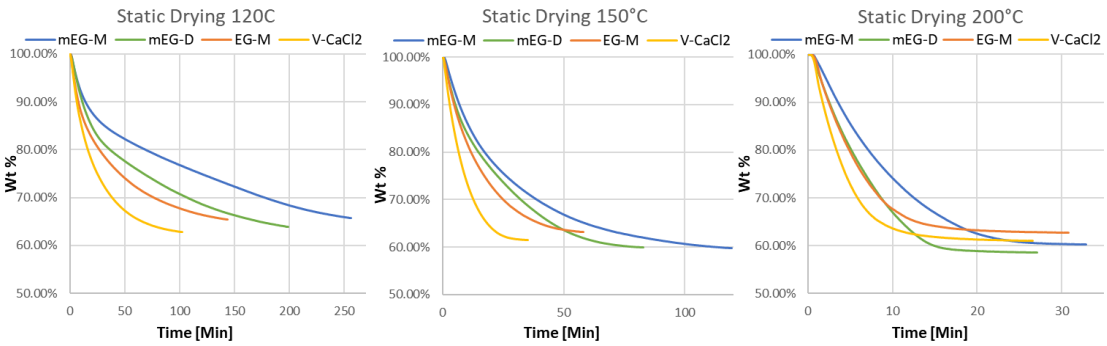

Fig. 9: Static Drying of 5g of material in the Ohaus MB120.

5. Conclusion

The successful synthesis of various EG/Alg based composites containing calcium chloride are presented. The synthesis method allows easy flexibility in size, shape, and material quantity to best suite the application at hand. Here we have used the Mould method to synthesis repeatable spherical beads of 6mm or the Drop-cast method to make beads between 3-4mm. Both methods offer a higher salt wt% than previously studied V-$CaCl_2$, achieving a maximum of 84% in the mEG-M sample. The spherical shape allows for good packing density achieving high salt volumetric densities. This is key when these materials are to be considered for transportation and storage at a domestic scale. The spherical nature also allows for good air flow through the packed bed during discharge reactions. Whereas V-$CaCl_2$ tends to create a very moist bottom layer in a packed bed, the larger beads (mEG-M and EG-M) create a more homogenous uptake of water. The output of heat energy is very promising achieving results like that of V-$CaCl_2$ while having a far superior amount of un-released energy at the point where V-$CaCl_2$ is considered exhausted. As for the dehydration process V-$CaCl_2$ performs better at small scale (5g) which is a comparison in terms of mass. To further assess the charge performance materials should be analyzed at a larger scale in volumetric terms. The superior air flow and salt volumetric densities should lead to better charge efficiency in the beads. At a larger scale, charge reactions might only be possible using a heat exchanger where heat transport will be key. For this, thermal conductivity studies should be conducted on materials. The benefit of using EG/Alg materials is that size and shape can be altered to improve these results.

Both synthesis methods can be easily upscaled to commercial use due to the simple and scalable synthesis routes. As well as this only cheap, abundant, and non-toxic materials are utilised. To further this work towards a point of real heat storage, larger scale tests should be conducted whereby sufficient cyclability should be significant goal. A common problem with salt hydrates is their ability to deliquesce. If this could be prevented or contained, material stability over time could be improved.

6. References

Barreneche, C., Fernández, A.I., Cabeza, L.F., Cuypers, R., 2015. Thermophysical characterization and thermal cycling stability of two TCM: CaCl2 and zeolite. Applied Energy. 137, 726–730. doi: 10.1016/j.apenergy.2014.09.025.

Brancato, V., Gordeeva, G,L., Capri, A., Grekova, A,D., Frazzica, A., 2021. Experimental comparison of innovative composite sorbents for space heating and domestic hot water storage. Crystals, 11, 5. doi: 10.3390/cryst11050476.

Casey, S. P., Aydin, D., Riffat, S., Elvins, J., 2015. Salt impregnated desiccant matrices for "open" thermochemical energy storage - Hygrothermal cyclic behaviour and energetic analysis by physical experimentation. Energy and Buildings. Elsevier B.V. 92, 128–139. doi: 10.1016/j.enbuild.2015.01.048.

Clark, R., Mehrabadi, A. and Farid, M. (2020). State of the art on salt hydrate thermochemical energy storage systems for use in building applications. Journal of Energy Storage. Elsevier. 27, 101145. doi: 10.1016/j.est.2019.101145.

Climate Change Act 2008 (no date) c. 27. Statute Law Database. https://www.legislation.gov.uk/ukpga/2008/27/section/1. Accessed July 2022.

Courbon, E., D'Ans, P., Permyakova, A., Skrylnyk, O., Steunou, N., Degrez, M., Frère, M., 2017. A new composite sorbent based on SrBr2 and silica gel for solar energy storage application with high energy storage density and stability. Appl. Energy. 190, 1184–1194. doi: 10.1016/j.apenergy.2017.01.041.

Gaeini, M., Rouws, A.l., Salari, J.W.O., Zondag, H.A., Rindt, C.C.M., 2018. Characterization of microencapsulated and impregnated porous host materials based on calcium chloride for thermochemical energy storage. Applied Energy. 212, 1165-1177. doi: 10.1016/j.apenergy.2017.12.131.

Jarimi, H., Aydin D., Yanan, Z., Ozankaya, G., Chen, X., Riffat, S., 2019. Review on the recent progress of thermochemical materials and processes for solar thermal energy storage and industrial waste heat recovery. International Journal of Low-Carbon Technologies. Oxford University Press. 44–69. doi: 10.1093/ijlct/cty052.

Kallenberger, P. A., Fröba, M., 2018. Water harvesting from air with a hygroscopic salt in a hydrogel–derived matrix. Communications Chemistry. Springer US. 1(1), 6–11. doi: 10.1038/s42004-018-0028-9.

Kallenberger, P.A., Posern, K., Linnow, K., Brieler, F.J., Steiger, M., Fröba, M., 2018. Alginate-Derived Salt/Polymer Composites for Thermochemical Heat Storage. Adv. Sustain. Syst. 2, 1700160. doi: 10.1002/adsu.201700160.

Krese, G., Koželj, R., Butala, V., Stritih, U., 2018. Thermochemical seasonal solar energy storage for heating and cooling of buildings. Energy and Buildings. 164, 239-253. doi: 10.1016/j.enbuild.2017.12.057.

Krönauer, A., Lävemann, E., Brückner, S., Hauer, A., 2015. Mobile sorption heat storage in industrial waste heat recovery. Energy Procedia, 2015. 73, 272-280. doi: 10.1016/j.egypro.2015.07.688.

Mohapatra, D., Nandanavanam, J., 2002. Salt in matrix for thermochemical energy storage - A review. Materials Today: Proceedings. Elsevier Ltd. doi: 10.1016/j.matpr.2022.05.453.

Morishige, K., Tateishi, N., 2003. Adsorption hysteresis in ink-bottle pore. The Journal of Chemical Physics. 119, 2301. doi: 10.1063/1.1585014.

Ofgem (2016). The Decarbonisation of Heat. Ofgem's Future Insights Series. https://www.ofgem.gov.uk/system/files/docs/2016/11/ofgem_future_insights_programme_-_the_decarbonisation_of_heat.pdf. Accessed July 2022.

Ofgem (2020). Ofgem Decarbonisation Action Plan. Ofgem. https://www.ofgem.gov.uk/system/files/docs/2020/02/ofg1190_decarbonisation_action_plan_revised.pdf. Accessed July 2022.

Salviati, S., Carosia, F., Saracco, G., Fina, A., 2019. Hydrated Salt/Graphite/Polyelectrolyte Organic-Inorganic Hybrids for Efficient Thermochemical Storage. Nanomaterials. 9(3), 420. doi: 10.3390/nano9030420.

Salviati, S., Carosia, F., Cantamessa, F., Medina, L., Berglund, L.A., Saracco, G., Fina, A., 2020. Ice-templated nanocellulose porous structure enhances thermochemical storage kinetics in hydrated salt/graphite composites. Renewable Energy. Elsevier Ltd. 160, 698–706. doi: 10.1016/j.renene.2020.07.036.

Sutton, R., Jewell, J., Searle, J., Elvins, J., 2018. Discharge performance of blended salt in matrix materials for low enthalpy thermochemical storage. Applied Thermal Engineering. Elsevier. 145, 483–493. doi: 10.1016/j.applthermaleng.2018.09.052.

Walsh, S., Reynolds, J., Abbas, B., Woods, R., Searle, J., Jewell, E., Elvins, J., 2020. Assessing the dynamic performance of thermochemical storage materials. Energies. 13(9). doi: 10.3390/en13092202.

Zhang, Y.N., Wang, R.Z., Li, T.X., 2018. Thermochemical characterizations of high-stable activated alumina/LiCl composites with multistage sorption process for thermal storage. Energy. 156, 240-249. doi: 10.1016/j.energy.2018.05.047.